Ammonium Polyphosphate/Montmorillonite Nanocompounds in Polypropylene

Deqi Yi, Rongjie Yang

National Laboratory of Flame Retardant Materials, School of Materials Science and Engineering, Beijing Institute of Technology, Beijing 100081, People's Republic of China

Received 11 April 2009; accepted 17 February 2010
DOI 10.1002/app.32362
Published online 26 May 2010 in Wiley InterScience (www.interscience.wiley.com).

ABSTRACT: Ammonium polyphosphate (APP)/montmorillonite (MMT) nanocompounds were prepared. The crystal forms and morphologies of the nanocompounds were studied by XRD, FTIR, SEM, and TEM. The APP/MMT nanocompounds were applied to intumescent flame-retarded polypropylene (PP) composites. The PP composites were studied by using oxygen index measurements, UL-94 flame testing, thermogravimetric analysis, and mechanical measurement. It was found that the APP/MMT nanocompounds enhanced the flame retardancy of the IFR/PP compared with the form II APP and its mixture with micro-MMT. © 2010 Wiley Periodicals, Inc. J Appl Polym Sci 118: 834–840, 2010

Key words: ammonium polyphosphate; montmorillonite; nanocompound; flame retardancy

INTRODUCTION

Ammonium polyphosphate (APP) is an important inorganic flame retardant. The basic formulation of an intumescent flame retardant (IFR) consists of APP, pentaerythritol (PER), and melamine (MA). When the flame-retarded polymer materials combust, the IFR forms a foaming char layer which insulates the bulk of the material from heat and oxygen, depresses smoke, and prevents melt dripping. To enhance the IFR, many researchers have combined it with metal salts,[1] metal oxide,[2] zeolite,[3] sepiolite,[4] and montmorillonite[5] to synergize the flame retardancy.

Montmorillonite (MMT) is a multilayered aluminosilicate clay with sodium counter-ions between the layers. The space between the clay layers is referred to as the clay gallery. To make it compatible with organic polymers, the sodium counter-ions are usually ion-exchanged with organic ammonium or phosphonium salts. The polymer/MMT nanocomposites may be prepared by blending or by polymerization. In the nanocomposites, the clay layers disperse by either intercalation or exfoliation. The MMT particles very often exist in the polymer materials at micron size; true nanoscale dispersion of the clay cannot be obtained because of its immiscibility with the polymer.

Polymer/MMT nanocomposites are useful both in decreasing the peak heat release rate and enhancing the material's mechanical properties. There are mainly three kinds of mechanisms in explaining the enhanced flame retardancy of the nanocomposites: a barrier mechanism,[6] radical trapping caused by iron or other paramagnetic impurities in the clay,[7] and catalytic effect on char formation.[8] The radical trapping process seems to be important only at low clay concentration; as the proportion of clay increases, the barrier mechanism dominates. The catalytic effect was researched recently. It played important role in some polymer/clay nanocomposites. Such as poly[ethylene-*co*-(vinyl acetate)]/organically modified MMT (OMMT),[8] and polyamide 12 (PA12)/OMMT nanocomposites.[9] Nanocomposites have also been observed to decrease the permeability of polymers.[10]

As a rule, APP particles disperse in the flame-retarded polymers at micron size, whereas MMT disperses in polymers at nano-size. This then raises the question: what would be the result of adding MMT nanodispersed in APP (i.e., an APP/MMT nanocompound) to polymers? Accroding to the self-assembly of alkylammonium chains on MMT,[11] it was thought possible that APP would self-assemble on MMT to produce an APP compound with nano-MMT. We, therefore, prepared APP/MMT nanocompounds[12] and applied them to polypropylene (PP) composites with the aim of improving flame retardancy.

EXPERIMENTS

Preparation

Seven types of APP/MMT nanocompound (n-AM) were prepared by heating diammonium hydrogen phosphate, phosphorus pentoxide, and urea in the

Correspondence to: R. Yang (yrj@bit.edu.cn).

TABLE I
Composition of n-AM and m-AM10 Samples

Samples	n-AM1	n-AM3	n-AM5	n-AM8	n-AM10	n-AM15	n-AM20	m-AM10
MMT wt %	1	3	5	8	10	15	20	10
APP wt %	99	97	98	92	90	85	80	80

molar ratios 1 : 1 : 0.3, then combined with different amounts of NaMMT (Nanocor Inc., Aberdeen, MS) in a well-covered kneading reactor and heated at a rate of between 10 and 20°C/min. When the reaction temperature reached ~ 250°C, dry ammonia was introduced. The ammonia atmosphere inside the reactor was then maintained at 300°C under constant pressure for 90 min, then cooled to below 150°C to obtain n-AM.[12] Depending on the different amounts of MMT used, seven APP/MMT nanocompounds were obtained: see Table I. They are referred to as n-AM1, n-AM3, n-AM5, n-AM8, n-AM10, n-AM15, and n-AM20, respectively. Their average particle size was 40 μm.

A type of crystalline form II APP (APP-II) of average particle size 15 μm was supplied by Hangzhou JLS Co. A simple mixture of the APP-II with micro-MMT was used as a reference sample, termed "m-AM10" in Tables I, II, V, and VI.

After combining with dipentaerythritol (DPER) and melamine (MA), the n-AM5, n-AM10, APP-II, and m-AM10 were blended with PP in a screw extruder. Then, the samples were molded by an injection machine (HTF80X 1 injection molding machine). The total content of the flame retardants was 20 wt % in the PP as shown in Table II.

Characterization

Powder X-ray diffraction data were collected by an X'Pert PRO MPD diffractometer with Cu $K\alpha_1$ radiation using a step size of 0.033 (2θ) and a counting time of 20 s/step. FTIR spectra of APP were collected by the attenuated total reflectance method of infrared spectrophotometry using a Nicolet 6700 spectrometer. Scanning electron microscope (SEM) images were taken using a Hitachi ultra-high resolution S4800 FE-SEM.

Limiting oxygen index (LOI) was measured using an oxygen index instrument (Rheometric Scientific Ltd., Piscataway, NJ) and according to the China national standard (GB/T 1406–1993). Mechanical properties were obtained using an Instron DXLL-5000 tensile testing machine and according to the China national standard (GB/T 1040.2-2006), at the 95% confidence level. Thermogravimetric analysis (TGA) was performed on a Netzsch F209 instrument under a flowing nitrogen atmosphere at a scan rate of 10°C/min from 40 to 800°C for the n-AM samples and from 40 to 600°C for the PP composites.

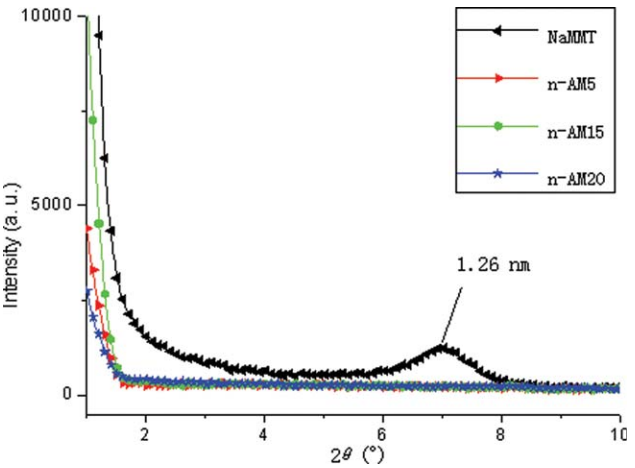

Figure 1 XRD patterns of NaMMT and n-AM samples. [Color figure can be viewed in the online issue, which is available at www.interscience.wiley.com.]

TABLE II
Composition of IFR/PP Samples

Sample	Molecular formula	PP/APP-II	PP/m-AM10	PP/n-AM5	PP/n-AM10
PP wt %	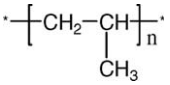	80	80	80	80
APP/MMT wt %	—	12	12	12	12
DPER wt %	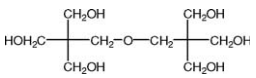	4	4	4	4
MA wt %	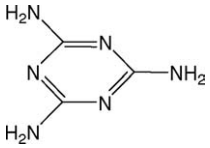	4	4	4	4

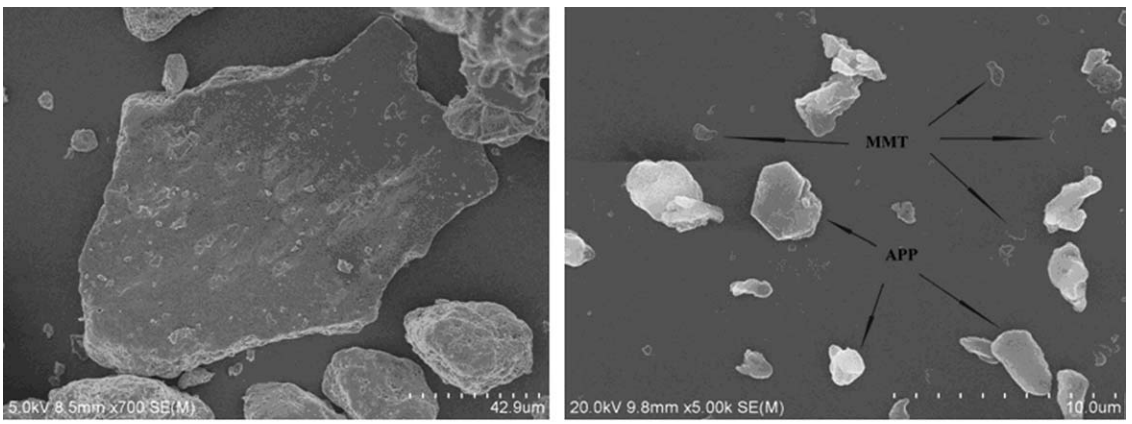

Figure 2 SEM images of n-AM5. (a) n-AM5 particle; (b) magnification of local surface, with APP particles and MMT sheets shown labeled.

RESULTS AND DISCUSSION

Structure of APP/MMT nanocompounds

The structure and apparent interlayer spacing (d-spacing) of the APP/MMT nanocompounds were detected by X-ray diffraction. Figure 1 shows the XRD patterns for NaMMT types n-AM5, n-AM15, and n-AM20. The spacing of the pristine NaMMT was calculated to be 1.26 nm from a diffraction peak at $2\theta = 7.04^\circ$ using the Bragg function. Three of the n-AM samples showed no diffraction peak in the 2θ range between 1° and 10°, implying that the MMT layers were exfoliated—that is, that the MMT was completely in the APP particles in those samples.

Figure 2 comprises two SEM images of the n-AM5 sample: 2(a) shows the surface of an n-AM5 particle containing dispersed MMT sheets; 2(b) is a magnified image of the local surface (continuous gray area) of the particle in 2(a), showing small APP particles and single MMT sheets (labeled).

The single MMT sheets in Figure 2(b) are parallel to the APP surface, and according to the ammonium head groups are positioned preferentially in the cavities of (Si-O) six-rings on the montmorillonite surface.[11] It was thought that there are main hydrogen bonds between APP chains and MMT sheets. Unluckly, we did not have enough data to prove that it is due to the self-assembly of the APP on the MMT sheets.

Figure 3 shows XRD patterns of seven of the APP/MMT nanocompound samples from 10° to 60°. It was noted that APP crystals transformed from form II to form I as the MMT content in the nanocompounds increased to 8 wt %, by which time the APP was nearly all form I crystal. Between 1 wt % and 8 wt % MMT, both forms were observed, indicating that the presence of MMT modified the

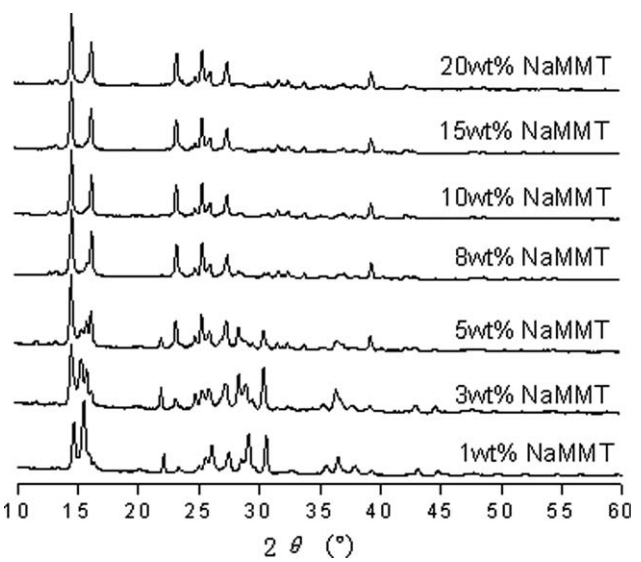

Figure 3 XRD patterns for the n-AM samples.

TABLE III
XRD Data for Form II and Form I APP

Form II APP			Form I APP		
2θ (°)	I/I_0	Diffracting plane (hkl)	2θ (°)	I/I_0	Diffracting plane (hkl)
14.68	45	002	12.84	9	210
15.53	100	022	13.24	4	–
22.21	12	101	14.68	100	220
25.65	8	102	16.37	70	040
26.11	25	111	23.33	50	211
27.51	18	020	24.85	14	410
29.16	40	112	25.46	45	041
30.60	30	103	25.99	25	420
35.63	10	121	27.52	30	430
36.53	16	104	32.53	14	421
37.98	10	122	33.88	15	431
			37.15	12	600
			39.29	30	630

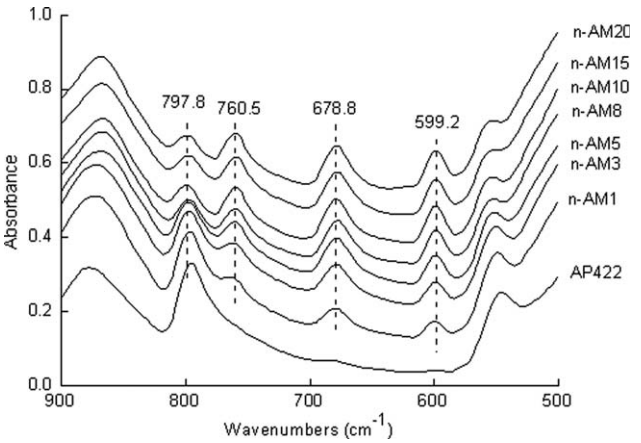

Figure 4 FTIR spectra of the n-AM and AP422 samples.

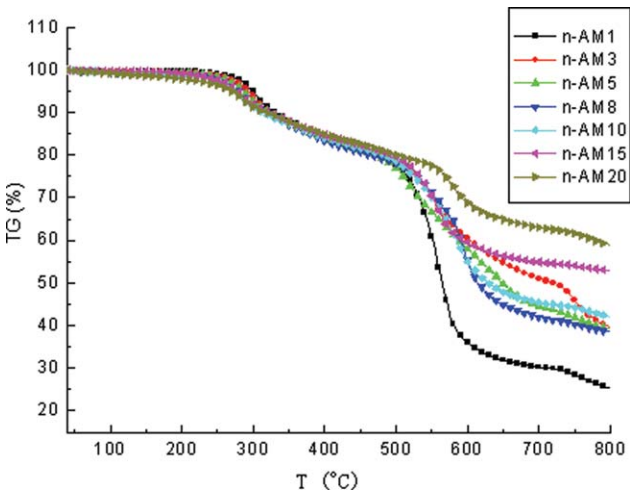

Figure 5 TGA curves for n-AM samples. [Color figure can be viewed in the online issue, which is available at www.interscience.wiley.com.]

crystal forms of APP. The XRD data for forms I and II APP are listed in Table III.

The FTIR spectra[13,14] for APP-I and APP-II crystals show absorbance peaks corresponding to phosphate at wavenumbers approximating to 1250 cm^{-1} for P═O bonds, and at 1010 and 1070 cm^{-1} for P—O bonds. The characteristic absorbances for APP-I are at 760, 660, and 602 cm^{-1}; the form II APP absorbance for the P—O—P bond occurs at 800 cm^{-1}.

Figure 4 shows the FTIR spectra for the seven n-AM samples of this study along with a commercially produced APP-II, AP422 (Clariant Co., Basel, Switzerland) for wavenumbers from 500 to 900 cm^{-1} measured using the attenuated total reflection method. As AP422 is a form II crystalline APP, it has no absorbances at wavenumbers 760.5, 678.8, or 599.2 cm^{-1}, but the seven n-AM samples show enhanced absorbance in the vicinity of these wavenumbers with increased MMT content. Beyond this point, the absorbance at about 797.8 cm^{-1} decreases with increased MMT content.

This suggests that the presence of the MMT layers in the n-AM samples preferentially produced crystal form I APP, at the same time inhibiting production of crystal form II.

Thermal stability of APP/MMT nanocompounds

Figure 5 shows TGA curves for the n-AM samples. It was observed that thermal degradation of the n-AM samples occurred in two main steps: the first from 300 to 500°C, the second above 500°C.

Table IV summarizes the 5% weight loss ($T_{5\%}$) and 35% weight loss ($T_{35\%}$), the final residual mass and the net residual mass (deducting the mass of MMT) at 800° C. In the first step, $T_{5\%}$ decreased with increasing MMT content; in the second stage, $T_{35\%}$ increased with increasing MMT content. It is notable that the n-AM20 showed an increase in the thermal degradation temperature at the second step, and its residual mass at 800°C increased with increasing MMT content.

According to earlier studies,[15,16] in the first step, APP mainly loses ammonia and water to form polyphosphoric acid; in the second step it mainly loses phosphoric acid fragments. In this study, it seems that the presence of MMT accelerated the first-step degradation (loss of ammonia and water) and decelerated the second step degradation (loss of phosphoric acid fragments).

Figure 6 shows TGA curves for the n-AM10, m-AM10, and APP-II samples. $T_{5\%}$ of the n-AM10 was 276.3°C, 20°C lower than m-AM10 and APP-II. However, it was noted that $T_{35\%}$ of the n-AM10 was 570.1°C, 40°C higher than APP-II value. In the second stage (500–800°C), the rate of weight loss for the n-AM10 is seen to have been lower than for the other samples, and the rate of weight loss for m-AM10 lower than that for APP-II. The final residual mass for n-AM10, m-AM10, and APP-II at 800°C

TABLE IV
TGA Data for n-AM Samples

Samples	n-AM1	n-AM3	n-AM5	n-AM8	n-AM10	n-AM15	n-AM20
$T_{5\%}$ (°C)	299.8	293.8	287.0	280.5	276.3	277.3	269.3
$T_{35\%}$ (°C)	543.1	572.0	559.4	578.7	570.1	566.1	646.8
Residual mass (%)	25.45	39.68	39.27	38.53	42.18	52.86	59.02
Net residual mass (%)	24.45	36.68	34.27	30.53	32.18	37.86	39.02

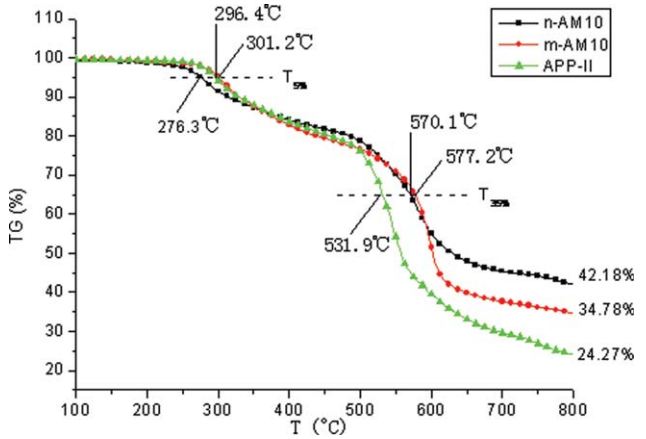

Figure 6 TGA curves for n-AM10, m-AM10, and APP-II. [Color figure can be viewed in the online issue, which is available at www.interscience.wiley.com.]

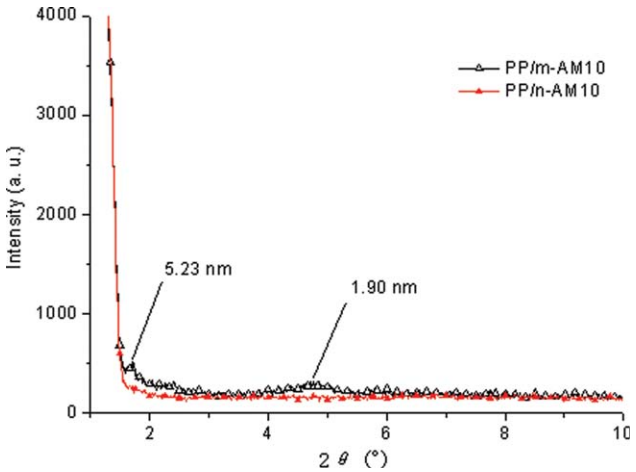

Figure 8 XRD patterns for PP/n-AM10 and PP/m-AM10. [Color figure can be viewed in the online issue, which is available at www.interscience.wiley.com.]

were 42.18%, 34.78%, and 24.27%, respectively. This again suggests that the loss of phosphoric acid fragments was decelerated by the presence of MMT, especially when the MMT was nanodispersed in the APP.

Flame-retarded PP by APP/MMT

Figure 7 shows SEM images of PP/n-AM10 and PP/m-AM10. In Figure 7(a), the particle size of the n-AM10 dispersed in PP is shown to be 10–50 μm; Figure 7(b) shows the particle size of APP-II to be 5–20 μm, smaller than the n-AM10 particles. Both of these size ranges indicate that the APP particles were microdispersed in the PP.

Figure 8 shows the XRD patterns for PP/n-AM10 and PP/m-AM10. The spacing of the MMT layers in the PP/m-AM10 was calculated to be 1.90 nm and 5.23 nm from the diffraction peaks at $2\theta = 4.74^\circ$ and 1.72°, respectively. There is no diffraction peak in the XRD curve for the PP/n-AM10, indicating that the MMT was exfoliated and nanodispersed in the APP, that is to say in the PP.

Figure 9 shows transmission electron microscope (TEM) images of the binary PP/n-AM10 composite. Figure 9(a) shows that the n-AM10 particles were microdispersed in the PP: an n-AM10 particle is circled. Figure 9(b) shows the exfoliated MMT sheets to be well dispersed within APP particles. No exfoliated MMT sheets were found to have transited into the PP matrix.

These results all indicate that the MMT was nanodispersed within the n-AM particles, but the PP/n-AM10 remained microcomposite.

The n-AM, m-AM, and pure APP combined with DPER and MA were used to produce flame-retarded PP. The APP/DPER/MA was added to the PP at the rate of 20 wt %. Table V lists the flame retardancies and mechanical properties for the PP composites with different APP.

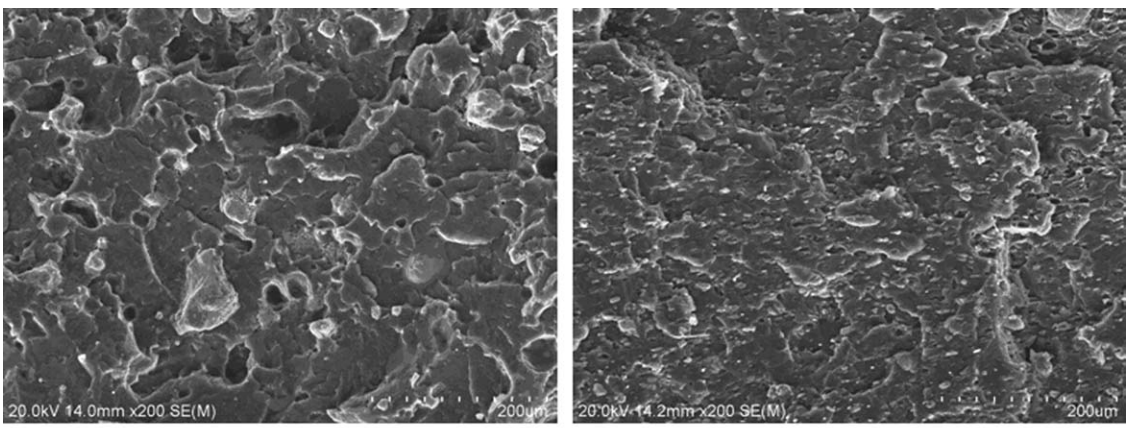

Figure 7 SEM images of PP/n-AM10 and PP/m-AM10. (a) PP/n-AM10; (b) PP/m-AM10.

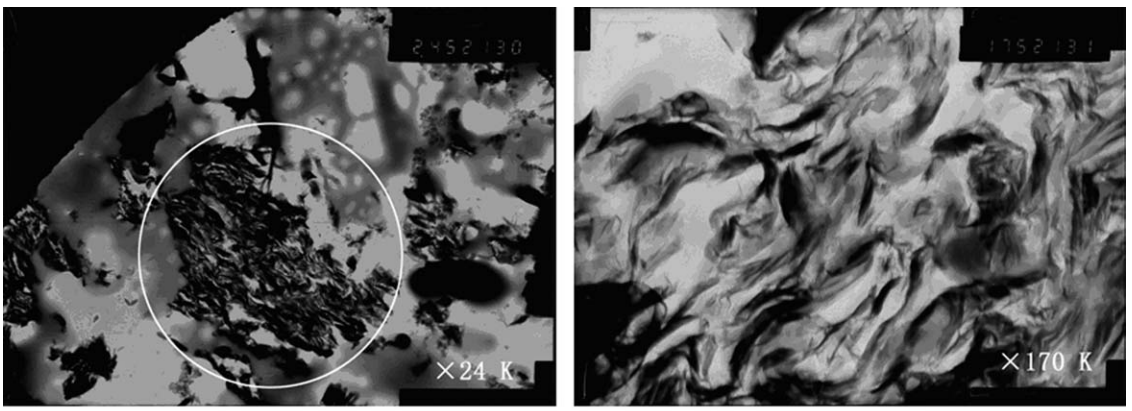

Figure 9 TEM images of the PP/n-AM10 composite. (a) n-AM10 particle in PP; (b) MMT sheets in n-AM10 particle.

It was noted that both the nano- and micro-sized MMT in the APP increased the LOI, while the LOI values with the n-AM were a little higher than with the m-AM. In particular, the samples containing n-AM10 reached the V-0 level in the UL-94 flame test (3.2 mm). In addition, the tensile strength and elastic modulus of each of the four samples were similar.

In Figure 10, TGA curves of the IFR/PP samples and pure PP are plotted; the 10% and 80% weight losses are abbreviated to $T_{10\%}$ and $T_{80\%}$. Table VI summarizes the final residual mass and the net residual mass of the PP samples.

Figure 10 and Table VI show that the early decomposition temperatures of the IFR/PP were reduced compared to that with the pure PP, but subsequent decomposition of the IFR/PP samples was retarded, especially when n-AM was used in the IFR.

In the PP/IFR composites, APP/MMT nanocompounds intensify the flame retardancy, for example by increasing the LOI and the amount of residue in TGA and making the composite reach the V-0 grade in the UL-94 test.

Under combustion APP/MMT nanocompounds release NH_3 and H_2O in the PP/IFR, which could increase the LOI; then, the nano-MMT layers play a part in the cross-linking structure formed by polyphosphoric acid and organic carbon and make the char more stable, insulating the bulk of the material from heat and oxygen. This is one of the reasons why the IFR/PP containing n-AM10 had a larger and more stable residual mass which enabled it to perform better in the UL-94 V-0 flame test (3.2 mm) than did the IFR/PP containing m-AM10.

Mechanism analysis

In preparing APP through diammonium hydrogen phosphate, phosphorous pentoxide, and urea, the crystal form II of APP was obtainable under normal reaction conditions. However, when the nano-MMT was in the system, only form I crystal APP was produced. It was also known that the form II APP is more complete and less defective than the form I APP. These findings indicate that there is a strong interaction between the APP chain and the nano-MMT layer in APP/MMT nanocompounds.

Judging from the TGA curves of the APP/MMT nanocompounds, APP-II and its mixture with micro-MMT, loss of NH_3 and H_2O from APP chains was accelerated but late degradation of polyphosphoric acid was inhibited to a certain extent by the nano-MMT layers; the micro-MMT in the mixture with APP-II influenced only the late degradation of polyphosphoric acid with limited surface area of micron particles.

This might suggest that surface ions on the nano-MMT layers may complex with the oxygen in P═O and P—O groups, weakening —O-NH_4^+ and —OH bonding and making the APP lose NH_3 and H_2O more easily. Consequent to the APP losing its NH_3 and H_2O, the nano-MMT layers promote formation of a polyphosphoric acid cross-linking network,

TABLE V
Flame Retardancy and Mechanical Properties of PP Composites with Different APP

PP composites	APP-II	m-AM10	n-AM5	n-AM10
UL-94 rate (3.2 mm)	NR	V-1	V-1	V-0
LOI (%)	25.9	29	29.7	29.8
Tensile strength (MPa)	31.1 ± 0.3	29.9 ± 0.5	29.7 ± 0.4	30.0 ± 0.4
Elastic modulus (MPa)	966.0 ± 17.4	976.8 ± 23.2	982.0 ± 15.2	998.7 ± 14.5

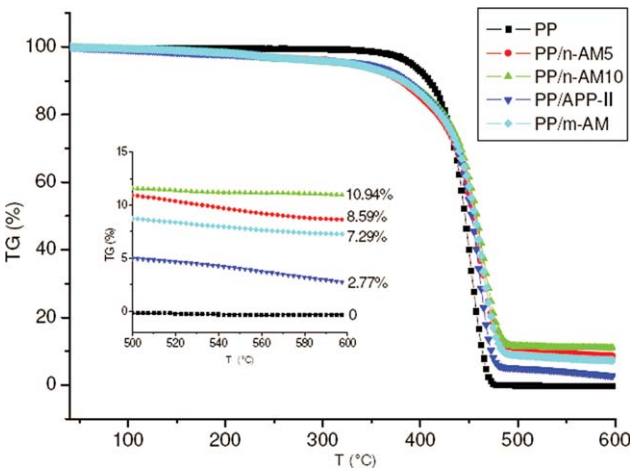

Figure 10 TGA curve for IFR/PP composites. [Color figure can be viewed in the online issue, which is available at www.interscience.wiley.com.]

which in turn inhibits polyphosphoric acid degradation and increases the amount of residue.

CONCLUSIONS

The APP/MMT nanocompounds were prepared through reaction of diammonium hydrogen phosphate, phosphorous pentoxide, and urea with addition of NaMMT clay. The microscopic structure of the APP/MMT nanocompounds was characterized using FTIR, XRD, and SEM techniques. MMT was observed to be exfoliated in the nanocompounds and APP crystals were transformed from form II to form I with increasing MMT content.

Compared to the APP-II and its mixture with the micro-MMT, the nano-MMT layers in the APP/MMT nanocompounds accelerated the first-step decomposition but decelerated the second-step decomposition of APP. Synthetically, the nano-MMT layers enhanced the thermal stability of APP at high temperature, and the APP/MMT nanocompounds improved the thermal stability and flame retardancy of PP/IFR composites. These improvements are attributed to the strengthening effect of nano-MMT layers cross-linking polyphosphoric acid and organic carbon networks and making the char more stable to insulate the bulk of the material from heat and oxygen.

TABLE VI
TGA Data for IFR/PP Composites

PP composites	PP	APP-II	m-AM10	n-AM5	n-AM10
$T_{10\%}$ (°C)	409.1	385.8	382.3	379.9	384.1
$T_{80\%}$ (°C)	458.3	466.4	472.7	473.6	476.0
Residual mass (%)	0	2.77	7.29	8.59	10.94
Net residual mass (%)	0	2.77	6.09	7.99	9.24

References

1. Davies, P. J.; Horrocks, A. R.; Alderson, A. Polym Degrad Stab 2005, 88, 114.
2. Levchik, S. V.; Levchik, G. F.; Camino, G.; Costa, L.; Lesnikovich, A. I. Fire Mater 1998, 20, 183.
3. Bourbigot, S.; Bras, M. L.; Bréant, P.; Trémillon, J.; Delobel, R. Fire Mater 1998, 20, 145.
4. Tartaglione, G.; Tabuani, D.; Camino, G.; Moisio, M. Compos Sci Technol 2008, 68, 451.
5. Bras, M. L.; Bourbigot, S. Fire Mater 1998, 20, 39.
6. Gilman, J. W.; Kashiwagi, T. In Polymer-Clay Nanocomposites; Pinnavaia, T. J., Beall, G. W., Eds.; Wiley: New York, 2000; p 67.
7. Zhu, J.; Uhl, F. M.; Morgan, A. B.; Wilkie, C. A. Chem Mater 2001, 12, 4649.
8. Zanetti, M.; Kashiwagi, T.; Falqui, L.; Camino, G. Chem Mater 2002, 14, 881.
9. Wang, Z.; Du, X. H.; Song, R. J.; Meng, X. Y.; Jiang, Z. W.; Tang, T. Polymer 2007, 48, 7301.
10. Du, J.; Wang, J.; Su, S.; Wilkie, C. A. Polym Degrad Stab 2004, 83, 29.
11. Heinz, H.; Vaia, R. A.; Krishnamoorti, R.; Farmer, B. L. Chem Mater 2007, 19, 59.
12. Yang, R.; Yi, D. China Invention Patent, A nanocompound of ammonium polyphosphate with montmorillonite and its preparation, CN101348721-A, 2008.
13. Drevellea, C.; Lefebvrea, J.; Duquesnea, S.; Brasa, M. L.; Poutchb, F.; Voutersc, M. Polym Degrad Stab 2005, 88, 130.
14. Camino, G.; Luda, M. P. In Fire Retardancy of Polymers: The Use of Intumescence; Brasa, M. L., Camino, G., Bourbigot, S., Delobel, R., Eds.; The Royal Society of Chemistry, Woodhead Publishing, Ltd.: Cambridge, UK, 1998; p 48.
15. Camino, G.; Costa, L.; Trossarelli, L. Polym Degrad Stab 1984, 6, 243.
16. Camino, G.; Costa, L.; Trossarelli, L. Polym Degrad Stab 1985, 12, 203.